A Pilot Protection Scheme for Transmission Lines of Half-Bridge MMC-HVDC Grids Using Cosine Distance Criterion

Mohammad Farshad

***Abstract*-- One of the major challenges in half-bridge modular multilevel converter-based high-voltage dc (MMC-HVDC) grids is the rapid detection and isolation of short-circuit faults before converter blocking and the entire grid shutdown. With the advancement of the hybrid dc circuit breakers (HDCCBs) in the ultra-fast isolation of faults, a considerable part of the problem has been solved. In this paper, relying on the performance of these circuit breakers and using the cosine distance criterion, a new pilot protection scheme is designed and presented for detecting short-circuit faults in transmission lines of half-bridge MMC-HVDC grids. While this scheme requires a comparatively low sampling frequency, its fault detection speed is quite independent of fault resistance. Moreover, this protection has the correct performance for any fault location along the line under protection and is completely stable against all external faults. The results of the evaluations on a 4-bus test grid under different fault conditions confirm the correct, ultra-fast, stable, selective, and reliable performance of the proposed line protection scheme.**

***Index Terms*-- Distance measurement mathematics, HVDC transmission, modular multilevel converters, power grids, power system protection.**

I. Introduction

In recent years, modular multilevel converters (MMCs) have attracted attention more than other converters for the development of multiterminal high-voltage dc (HVDC) grids [1]. This type of converter has been introduced in various structures like half-bridge, clamped double half-bridge, and full-bridge; among which, the half-bridge MMC has less cost and losses [2], [3]. However, the half-bridge MMC is not able to control fault currents, and as a result, HVDC grids based on this type of converter face the challenge of the ultra-fast detection and interruption of short-circuit currents before converter blocking and the entire grid outage. Employing the hybrid dc circuit breakers (HDCCBs), faults can be isolated very fast [4]. Nevertheless, to detect faults rapidly and correctly, specific protection schemes should also be designed for these grids.

Among the schemes proposed for the protection of transmission lines in MMC-HVDC grids, some of them are based on local measurements in one terminal. For instance, the authors of [5] have utilized the locally measured voltage change rate for designing a quick-action protection scheme. The authors of [6] have also presented a single-ended protection scheme based on the voltage derivative and magnitude for detecting faults and the current derivative for determining their direction. In [7], the researchers have employed the voltage derivative as the start-up criterion, the voltage high-frequency transients for distinguishing internal faults, and the current changes for faulty pole selection. Some other criteria combinations used so far in the single-ended protection schemes are as follows: voltage derivative, difference of integral of voltage changes in positive and negative poles, and integral of square of transient voltages [8]; voltage derivative and integral of reactor voltage in 0 and line modes [9]; energy of coefficients obtained from real-time boundary wavelet transform of reactor voltages [10]; voltage drop and morphological gradient of voltage traveling-waves [11]; voltage derivative and energy of forward and backward traveling-waves [12]; wavelet transform modulus maximum of initial traveling-wave [13]; current derivative and wavelet transform modulus maximum of initial traveling-wave [14]; abrupt voltage change (for backup protection) [15]; and forward and backward traveling-waves' energies and time difference of traveling-waves in 0 and 1 modes [16]. Despite the innovative design of these schemes, they may suffer from some inherent shortcomings. For instance, the studies in [17] show that criteria like the current and voltage derivatives require a relatively high sampling frequency for acceptable performance. Also, the sensitivity of these single-ended protections may decrease for faults far from the measuring point [14], and they may require receiving the trip signal from the protection on the other end for such faults [16].

Another category includes the line protection algorithms that require signals measured at two or more points for calculations. For instance, the backup protection based on the voltage changes and the cosine similarity between forward and backward traveling-waves at both line terminals [18], the differential protection based on the wavelet transform and the energy of current signals at both line ends [19], and the differential protection based on the optical current sensors

Manuscript received November 27, 2019; revised February 18, 2020; revised April 14, 2020; accepted June 9, 2020.
The present work was financially assisted by the Gonbad Kavous University (assigned ID: 6-357).
M. Farshad is with the Department of Electrical Engineering, Faculty of Basic Sciences and Engineering, Gonbad Kavous University, Gonbad Kavous 49717-99151, Iran (e-mail: farshad@gonbad.ac.ir).

distributed along lines [20] fall into this category.

Third category comprises the line protection schemes that perform calculations at each end of the line based on local measurements; while, they require to exchange the fault detection signals between two ends for making the final protective decisions. The authors of [21] have designed primary and backup protections based on the locally measured voltage of current-limiting reactors, where the backup protection requires to share the fault detection signals between the protected line ends, via a communication link. Also, the researchers have employed the voltage polarities of current-limiting reactors in [22] and the voltage changes and the polarities of traveling-waves' transient energy in [23] to design the protections that require exchanging the binary fault detection logics as the results of local measurements and computations at each line terminal. It should be noted that transmitting and receiving logic signals with binary values of 0 or 1, rather than measured current and voltage signals, are technically simpler with lower processing delays and do not necessitate time synchronization. However, the speed of the protections in the third category still depends on the line length due to the time delay of fault signature arrival to both terminals and the communication latency. As noted by the authors of [22], their protection has been originally designed to back up the primary protection. On the other hand, the authors of [23] have discussed the applicability of their scheme as the primary or backup protection. Indeed, all the line protections presented in [21]-[23], even those originally designed to back up the primary protection, can satisfy the primary protection requirements if the line length is not too long [23].

In this paper, a new scheme based on the cosine distance criterion is proposed for protecting lines in half-bridge MMC-HVDC multiterminal systems, which belongs to the third category of the schemes. This ultra-high-speed protection requires a smaller sampling frequency in comparison to the existing ones, making its implementation easier. This scheme performs well for all fault locations along the line under protection, and its speed is independent of the fault resistance. Also, this protection is stable for all ac and dc faults outside the protected line.

The rest of this paper is prepared as follows: Section II analyzes line faults in MMC-HVDC grids. Section III describes the proposed scheme. The evaluation results are presented in Section IV. Lastly, this paper is concluded in Section V.

II. Analysis of Short-Circuit Faults in Grid Lines

Fig. 1 depicts a portion of a half-bridge MMC-HVDC grid with the symmetric monopole configuration embedding HDCCBs. Also, this grid is equipped with voltage and current measurement instruments between each HDCCB and its corresponding current-limiting reactor, L_{dc}. Suppose that a fault occurs on the positive pole of the transmission line between Buses k and j. As can be seen in Fig. 1, immediately after the fault occurs, the superimposed fault currents flow along the measurement direction at both sides of the faulty line and have increasing effects on both measured currents. On the other hand, the superimposed fault current in a healthy line flows along the measurement direction at one side and the opposite direction of the other one. Moreover, the superimposed fault voltages have significant decreasing effects on the measured voltages at both sides of the faulty line.

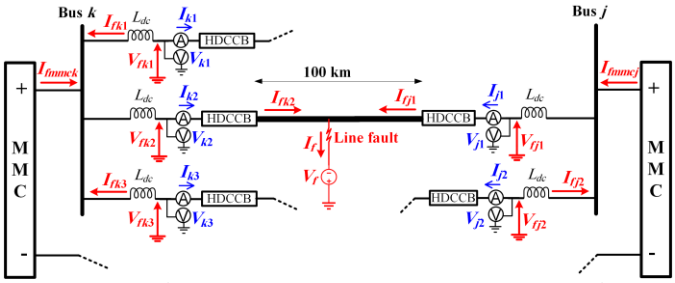

Fig. 1. A portion of a multiterminal MMC-HVDC system with a line fault.

The superimposed fault components at time t can be calculated by subtracting the prefault components from the measured values at time t:

$$I_{fkn}[t] = I_{kn}[t] - I_{Lkn} \tag{1}$$

$$V_{fkn}[t] = V_{kn}[t] - V_{Lkn} \tag{2}$$

where, I_{fkn}, I_{kn}, I_{Lkn}, V_{fkn}, V_{kn}, and V_{Lkn} are the superimposed current, the measured current, the average prefault load current, the superimposed voltage, the measured voltage, and the average prefault voltage, respectively, at the boundary of n^{th} transmission line linked to Bus k. By replacing index k with j in these variables, the corresponding values for the lines connected to Bus j are represented.

Figs. 2 and 3 exhibit the superimposed fault currents and voltages of the positive pole, respectively, for two positive-pole-to-ground (p-g) short-circuit faults in the 100-km line shown in Fig. 1 under the following conditions:

- At 10 km from Bus k with a 5-Ω fault resistance
- At 10 km from Bus j with a 100-Ω fault resistance

As can be seen in Fig. 2, in the first postfault moments, ignoring the amplitudes, the orientations of the fault current signals at both ends of the faulty line, I_{fk2} and I_{fj1}, are incremental and the same under different fault conditions, offering a discriminating criterion for detecting the faults on this line. Furthermore, as can be comprehended from Fig. 3, the superimposed voltage signals at both ends of the faulty line, V_{fk2} and V_{fj1}, have experienced significant drops, and their orientations are the same under both fault conditions. Although the voltage orientation does not offer a better discriminating criterion compared to the current orientation, it can be considered as an auxiliary criterion to be sure about the fault occurrence, for more reliably discriminating fault cases from other normal or abnormal conditions.

It should be noted that similar analysis results can be inferred for the faults occurring on the negative pole with attention to the measuring direction of the instruments installed on this pole.

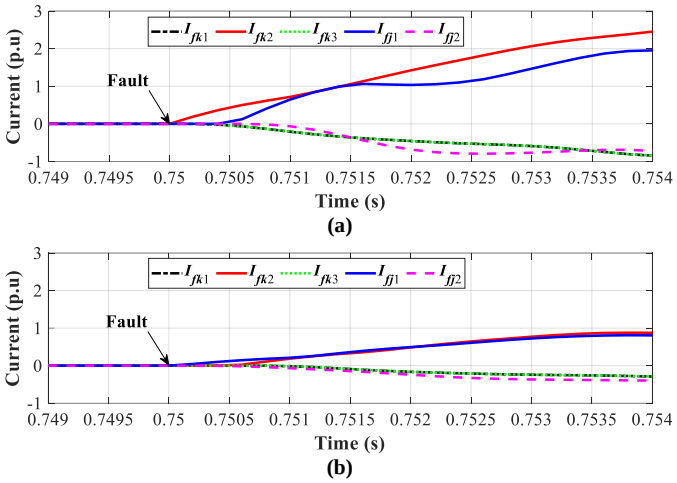

Fig. 2. Superimposed currents for faults: (a) at 10 km from Bus *k* with a 5-Ω fault resistance, (b) at 10 km from Bus *j* with a 100-Ω fault resistance.

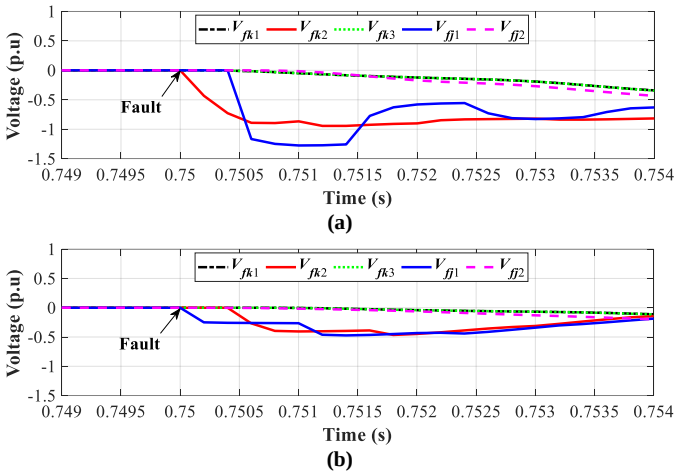

Fig. 3. Superimposed voltages for faults: (a) at 10 km from Bus *k* with a 5-Ω fault resistance, (b) at 10 km from Bus *j* with a 100-Ω fault resistance.

III. Line Protection Scheme

Based on the discussions provided in Section II, it is sensible to prerecord some reference superimposed signals under an internal fault condition and compare the orientations of real-time new superimposed signals to them for distinguishing possible internal faults. The cosine distance measure is suitable for this purpose since it can provide the quantitative orientation difference between two input vectors/signals [24], ignoring their amplitudes that can be affected by the location and resistance of faults. The greater the orientation difference, the greater the cosine distance value, and vice versa. Besides, the use of superimposed components will cancel out possible effects of prefault conditions on the scheme's performance. The cosine distance of each data window of a superimposed signal to the corresponding reference signal is calculated as follows:

$$d_C(X,Y) = 1 - \frac{\sum_{i=1}^{m}(\varepsilon + x_i)(\varepsilon + y_i)}{\sqrt{\sum_{i=1}^{m}(\varepsilon + x_i)^2}\sqrt{\sum_{i=1}^{m}(\varepsilon + y_i)^2}} \tag{3}$$

where, $d_c(.,.)$ indicates the cosine distance function, x_i is the i^{th} sample in the considered data window of the superimposed component X, y_i is the i^{th} sample of the corresponding reference signal Y, and m is the number of samples in the data window. The cosine distance d_c is generally a value between 0 and 2. To ensure that x_i and y_i are of the same sign under normal operating conditions, and consequently, the cosine distance remains between 0 and 1 and does not abruptly fluctuate under these conditions, the following ε is added to them:

$$\varepsilon = \alpha \times |y_{base}| \times \mathrm{sgn}\left(\sum_{i=1}^{m} y_i\right) \tag{4}$$

where, sgn(.) indicates the sign function, y_{base} is the grid base value for the signal of interest (current or voltage), and α is a small positive constant factor. The factor α should be chosen so that the absolute of ε is greater than the maximum magnitude of the corresponding superimposed values' deviations from zero in the normal operating conditions. Usually, taking α in the range 0.05~0.1 is sufficient to meet this stipulation. As can be comprehended from (4), the value of ε will be equal to a small proportion of the relevant nominal value, with a sign identical to the dominant sign of the relevant reference signal.

A. Designing Line Protection Algorithm

For generating the reference signals for the protection of each pole of each transmission line, first, a severe (solid) fault that has a high priority to be rapidly detected is applied in the middle of that line. Then, 2-ms data windows of the superimposed current and voltage signals at both line ends are recorded, including 1 ms ahead of and 1 ms later than the moment of fault signature appearance.

The protection units are located on both ends of the protected pole. In the protection unit of each side, at any moment, 2-ms data windows of the locally measured current and voltage signals at the beginning of the protected pole are considered as inputs. Then, the corresponding averages of 2-ms data windows just a moment ago, e.g., 16 ms ago, are subtracted from them so that the superimposed components are obtained. With attention to the quickness of protections and HDCCBs, this 16-ms delay is sufficient for correctly calculating the prefault components for the time frame required after the fault incidence.

In the next step, the cosine distances between the data windows of the superimposed components and the corresponding prerecorded reference signals are calculated and compared with the threshold values. For example, for the protection unit installed at the boundary of 2nd transmission line linked to Bus *k*, the following conditions are checked:

$$d_C\left(I_{fk2}^{w}, I_{fk2}^{ref}\right) < d_{Cthr}^{LI} \tag{5}$$

$$d_C\left(V_{fk2}^{w}, V_{fk2}^{ref}\right) < d_{Cthr}^{LV} \tag{6}$$

where, I_{fk2}^{w} and V_{fk2}^{w} are the vectors containing 2-ms data windows of the superimposed current and voltage signals, respectively, at the boundary of 2nd transmission line linked to

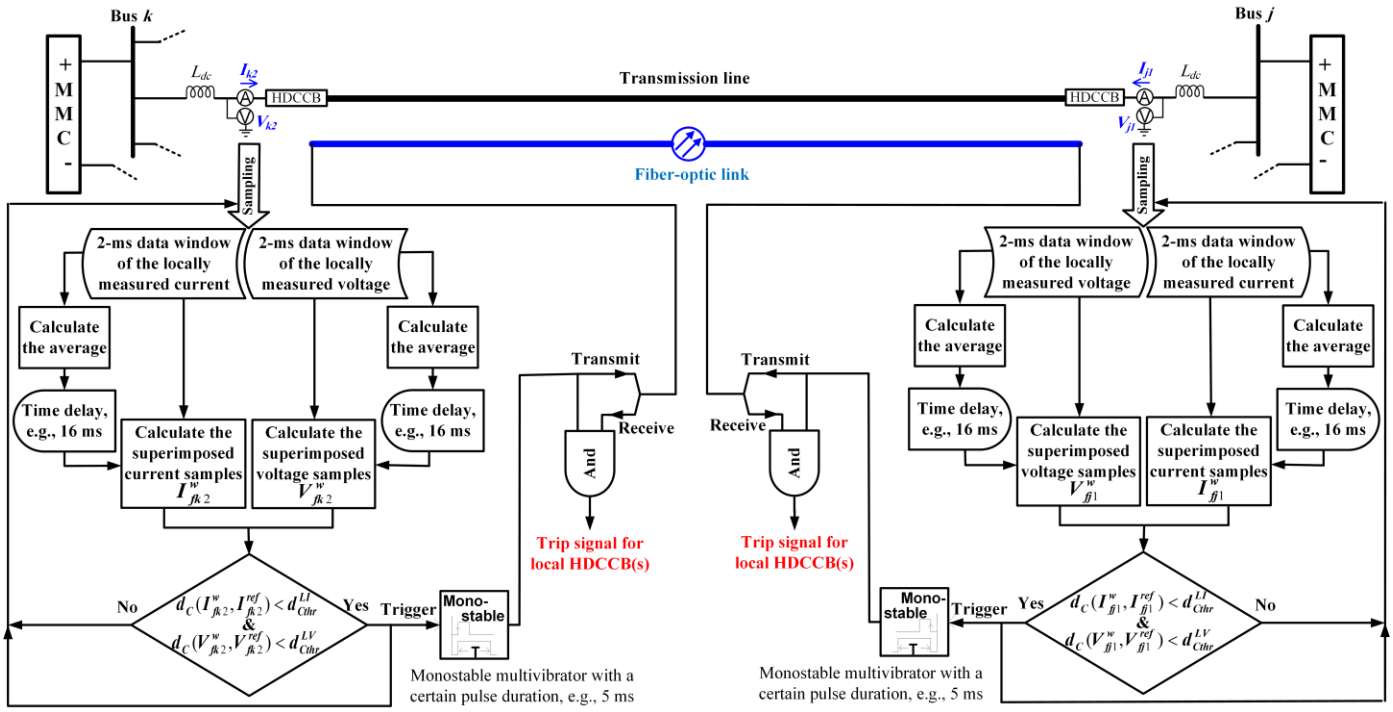

Fig. 4. Pilot protection algorithm designed for one pole of the transmission line between Buses *k* and *j*.

Bus *k*. Likewise, I_{fk2}^{ref} and V_{fk2}^{ref} indicate the vectors containing 2-ms data windows of the reference current and voltage signals, respectively, prerecorded at the boundary of 2nd transmission line linked to Bus *k*. Moreover, d_{Cthr}^{LI} and d_{Cthr}^{LV} are the thresholds of the line current and voltage cosine distances, respectively.

If both of the conditions (5) and (6) are simultaneously satisfied, a logic signal with a value of 1 is transmitted via a fiber-optic link to the protection unit of the other end for a certain duration of time, e.g., 5 ms, using a monostable multivibrator. This 5-ms pulse duration is considered to compensate for the time delay of fault signature arrival to the other side, the communication latency, and the detection time delay of the remote protection unit. If a signal indicating fault is also received from the other end of the pole during this 5 ms, the trip signal is generated. If the grid is bipolar, the trip command is issued to only the local HDCCB of the protected pole, while in a monopolar grid, the disconnection command should be sent to the local HDCCB of the opposite pole too [2]. Fig. 4 illustrates the line protection algorithm designed for one pole of the transmission line between Buses *k* and *j*.

In the proposed scheme, when the calculations designated in the algorithm are completed for the present data windows, the input data window of each measuring signal will be updated by entering one new sample and throwing out the last old sample.

The thresholds should be set for critical non-severe conditions. Hence, for adjusting the threshold values for the protection of each line, d_{Cthr}^{LI} and d_{Cthr}^{LV}, it is recommended to consider a non-severe internal fault condition, like a single-pole fault with a probable high resistance that is desirable to be quickly detected. It is also sensible to place this fault in the middle of the line for ensuring the applicability of the adjusted thresholds for the protection units located on both ends. Through investigating the obtained cosine distances in the postfault moments, the threshold values should be determined such that the protection units located on both ends of the protected pole can quickly detect this non-severe fault by simultaneously satisfying both the conditions (5) and (6).

B. Detection and Trip Time Delays

One of the important requirements of the protections designed for half-bridge MMC-HVDC grids is the detection of internal fault and the issuance of trip command within a few milliseconds, e.g., 3 ms for the *Zhangbei* grid in China [8], [14]. Fig. 5 illustrates a diagram of the scheme's time delays for a fault closer to Bus *k*. In this figure, t_k^{det}, t_k^{trp}, t_j^{det}, and t_j^{trp} indicate the fault detection delay in Bus *k*, the trip command delay in Bus *k*, the fault detection delay in Bus *j*, and the trip command delay in Bus *j*, respectively, after the appearance of fault signatures. Also, t_{kj}^{com} and t_{jk}^{com} are the delays regarding the transmission of fault detection signals between Buses *k* and *j*. Based on Fig. 5, the maximum trip delay at each end is related to the case in which a fault occurs in the closest distance from that end; because, in this case, the time delay of fault signature arrival to the other side is maximum; while, the fault signature appears immediately at that end.

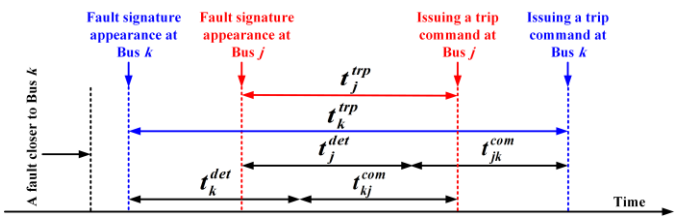

Fig. 5. Diagram of the proposed scheme's time delays.

IV. Results and Discussion

Here, the proposed scheme is evaluated on a test grid simulated in PSCAD/EMTDC interfaced with MATLAB.

A. Test Grid

Fig. 6 depicts the single-line diagram of the test 4-bus half-bridge MMC-HVDC grid with the symmetric monopole configuration and the rated voltage of ±320 kV [25]. The half-bridge MMCs are simulated based on the continuous model considering blocking capability. The rated powers of MMC1, MMC2, and MMC3 are 900 MVA, while the rated power of MMC4 is 1200 MVA. In this grid, each HDCCB is simulated based on a simplified model, including an ideal circuit breaker in parallel with an arrester with a rated voltage of 480 kV, which starts interrupting the current with a 2-ms delay after receiving the trip command. The series current-limiting reactor, L_{dc}, of each HDCCB has an inductance of 150 mH. The cable lines of the test grid are simulated based on the frequency-dependent model (phase) using the configuration presented in [25]. More details of this grid can be accessed in [25].

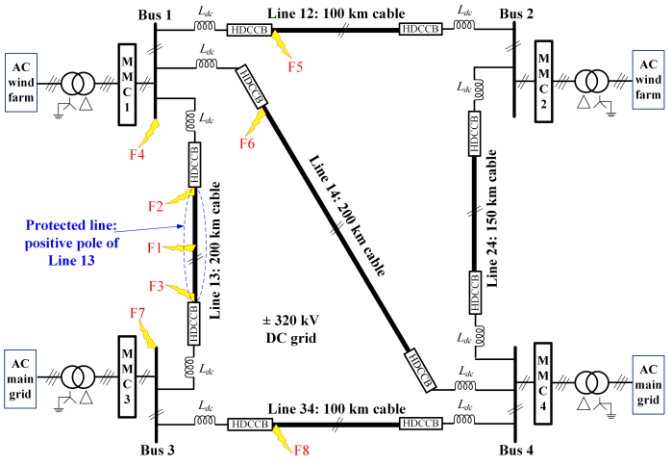

Fig. 6. Single-line diagram of the test grid.

B. Preparing the Line Protection

In this study, the proposed protection is only installed on two sides of the positive pole of the 200-km cable line between Buses 1 and 3, i.e., Line 13. The signals are sampled at 5 kHz. According to the measurement results in [26], the communication delay in the fiber-optic cable is about 5 μs/km. Thus, to simulate the communication delay in the 200-km fiber-optic cable between Buses 1 and 3, a 1-ms delay is considered for receiving the detection signal from the other side.

For generating the reference signals for the protection of the positive pole of Line 13, a positive-pole-to-negative-pole (p-n) short-circuit fault through a 0.01-Ω resistance is simulated in the middle of the line, and the superimposed current and voltage samples at both ends of the line are stored 1 ms before and after the fault signature appearance. Fig. 7 shows the recorded reference signals for this fault. As can be seen, since the prefault conditions are eliminated and the superimposed components are used, the reference signals of both ends are almost the same; while, the prefault values of one end differ from the other.

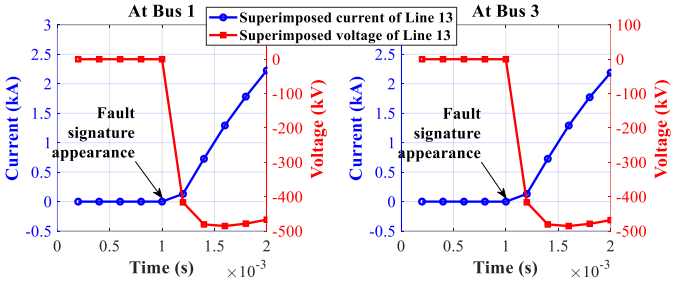

Fig. 7. Reference signals for the protection of the positive pole of Line 13.

To calculate ε using (4), α is considered to be 0.05 (the same for current and voltage). The base voltage of the grid is 320 kV. Also, considering the rated power of the largest converter, i.e., 1200 MVA, the base current of the grid is 1.875 kA.

For setting the thresholds of the line protection, a p-g short-circuit fault with a 500-Ω high resistance is simulated in the middle of Line 13. Fig. 8(a) presents the superimposed current and voltage signals of the positive pole, and Fig. 8(b) shows their cosine distance values relative to the corresponding reference samples. The threshold values should be determined such that the line protection can detect the fault as soon as possible. According to this figure, the thresholds, d_{Cthr}^{LI} and d_{Cthr}^{LV}, are determined as 0.2 and 0.15, respectively.

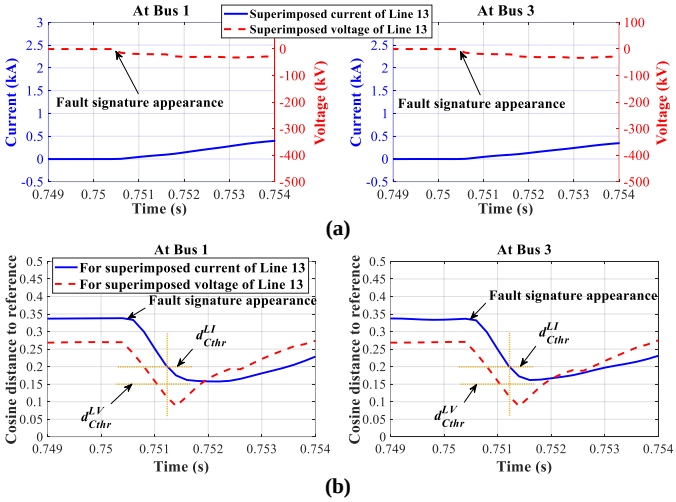

Fig. 8. Simulation of a p-g fault with a 500-Ω resistance in the middle of Line 13: (a) superimposed current and voltage signals, (b) cosine distances.

C. Performance for Internal Faults

Here, the protection of the positive pole of Line 13 is evaluated for internal p-n and p-g faults located at F1, F2, and F3 indicated in Fig. 6. As an example case, Fig. 9(a) exhibits the superimposed current and voltage signals of the positive pole, and Fig. 9(b) shows the cosine distances, the fault detection signals, and the trip signals on both ends of the protected line for the internal solid p-n fault at F2. As is clear in Fig. 9(b), the protection units of both ends have picked up and issued the trip commands correctly.

Table I represents the detection and trip time delays after the appearance of fault signatures, i.e., t_1^{det}, t_1^{trp}, t_3^{det}, and t_3^{trp}

indicated in Fig. 5, for various internal fault conditions. According to this table, the time delays do not depend on the fault resistance value. Indeed, the proposed line protection can detect p-g faults with resistance values up to 500 Ω and p-n faults with resistance values up to 1000 Ω very fast and issue the disconnection command to the local HDCCBs with a maximum delay of 3 ms. This maximum delay is related to the faults at the boundaries of the 200-km-long cable line. Thus, considering a typical allowable delay of 3 ms [8], [14], the proposed algorithm can properly act as the primary protection for cable lines with lengths up to 200 km. The proposed line protection can be employed as fast backup protection for longer cable lines due to the increased time delay of fault signature arrival to both terminals and the increased communication latency.

TABLE I
Performance of the Protection of Line 13 for Internal Faults

Fault location	Fault type	Fault resistance (Ω)	t_1^{det} (ms)	t_1^{trp} (ms)	t_3^{det} (ms)	t_3^{trp} (ms)
F1 (in the middle of Line 13)	p-g	0.01	0.8	1.8	0.8	1.8
		500	1.0	2.0	1.0	2.0
	p-n	0.01	0.8	1.8	0.8	1.8
		500	0.6	1.6	0.6	1.6
		1000	1.0	2.0	1.0	2.0
F2 (near Bus 1)	p-g	0.01	0.8	3.0	0.8	0.8
		500	0.8	3.0	0.8	0.8
	p-n	0.01	0.8	3.0	0.8	0.8
		500	0.6	2.8	0.6	0.6
		1000	0.8	3.0	0.8	0.8
F3 (near Bus 3)	p-g	0.01	0.8	0.8	0.8	3.0
		500	0.8	0.8	0.8	3.0
	p-n	0.01	0.8	0.8	0.8	3.0
		500	0.6	0.6	0.6	2.8
		1000	0.8	0.8	0.8	3.0

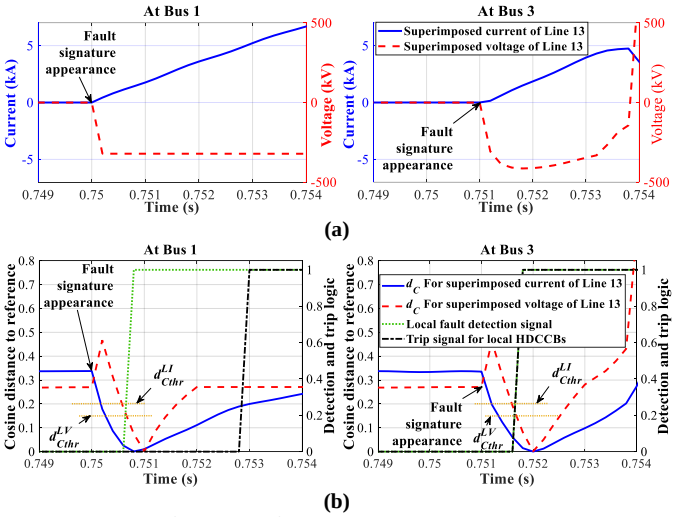

Fig. 9. Simulation of a solid p-n fault at F2: (a) superimposed signals, (b) cosine distances, detection signals, and trip signals.

D. Performance for External Faults

Here, the protection of the positive pole of Line 13 is evaluated for severe external faults. To this end, three solid p-n faults at Bus 1, at the beginning of Line 12, and at the beginning of Line 14, i.e., at F4, F5, and F6, are simulated. The obtained results show that the protection unit of Bus 3 sees and detects the external faults located at F4, F5, and F6; however, it does not issue the trip command because it does not receive the confirmation from the protection unit of Bus 1. As an example, Fig. 10 shows the simulation result for the external fault at F4, confirming the described operation for the protection units of Buses 1 and 3. For investigating the scheme's robustness, in the simulation of this external bus fault, it is supposed that the HDCCBs connected to Bus 1 are tripped by the bus protection [27] in a short time after the fault. According to Fig. 10(b), even when the HDCCBs connected to Bus 1 have started to open, the cosine distances in the protection unit of Bus 1 have not gone down lower than the thresholds simultaneously, and the protection have not maloperated.

For more investigations, two solid p-n faults at Bus 3 and at the beginning of Line 34, i.e., F7 and F8, are also simulated. According to the results, the protection unit of Bus 1 detects the external faults at F7 and F8; however, it does not issue the trip command because it does not receive the confirmation from the protection unit of Bus 3. As an example, Fig. 11 exhibits the simulation result for the external fault at F8. This figure also confirms the described operation for the protection units located on Buses 1 and 3 and the robustness of the proposed scheme.

Since the scheme is stable during the severe (solid) external faults, it will be logically robust against resistive ones as well.

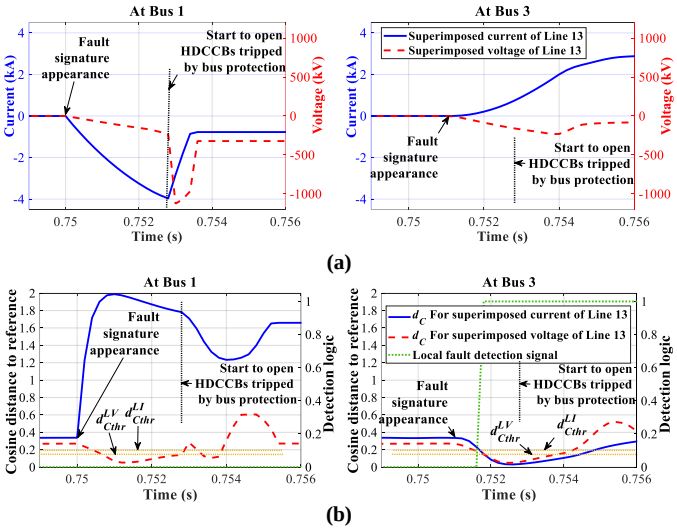

Fig. 10. Simulation of an external solid p-n fault at F4: (a) superimposed signals, (b) cosine distances and detection signals.

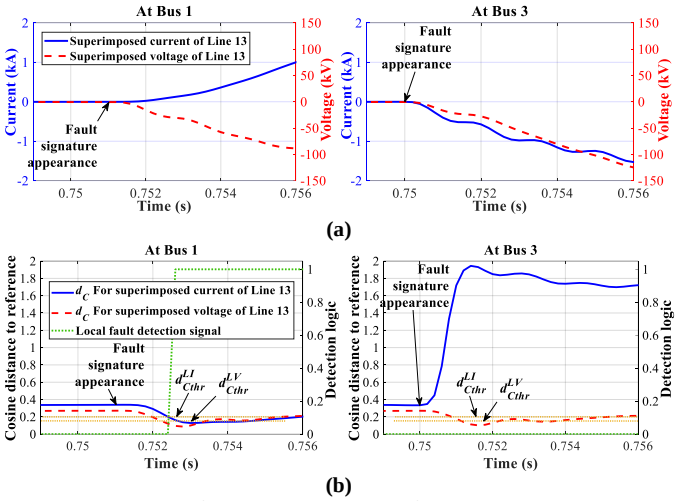

Fig. 11. Simulation of an external solid p-n fault at F8: (a) superimposed signals, (b) cosine distances and detection signals.

E. Performance under Measurement Errors

For studying the impacts of measurement errors on the scheme's performance, ±2.5% uniformly distributed random errors are added to the voltage and current samples measured at both ends of Line 13, while the protection thresholds and the reference signals are the same as before. Fig. 12 presents the cosine distances, the fault detection signals, and the trip signals on both ends of the protected line in the presence of measurement errors for in-zone p-n faults through a high resistance of 1000 Ω at F1 and through a low resistance of 0.01 Ω at F2. As can be seen, the protection units of both ends have successfully detected these faults and issued the trip commands. It should be noted that even with the measurement errors, the detection and trip time delays are the same as the ones presented in Table I.

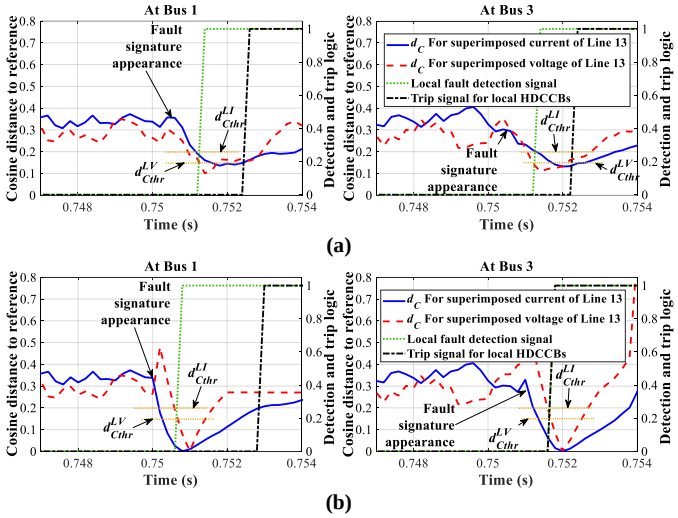

Fig. 12. Cosine distances, detection signals, and trip signals in the presence of measurement errors for internal p-n faults: (a) with a 1000-Ω high resistance at F1, (b) with a 0.01-Ω low resistance at F2.

F. Performance in Bipolar grids

Here, the ±320-kV symmetric monopole test grid described in Section IV.A is modified to a ±640-kV symmetric bipolar grid with the ground return [1]. Then, the same line protection prepared in Section IV.B is employed for protecting the positive pole of Line 13 in the modified bipolar grid as well. According to the results obtained in the case of internal and external faults, the performance of the proposed scheme in the modified bipolar grid is very similar to its performance in the monopole test grid.

As mentioned in Section III.A, the proposed protection scheme is separately implemented for each pole of each transmission line. The robustness of the protection of each pole against single-pole faults on the opposite pole can be one of the requirements, especially in bipolar grids. The evaluation results obtained in the modified bipolar grid confirm that the proposed scheme can remain stable during the faults involving only the opposite pole. As an example, Fig. 13 presents the simulation result for the solid negative-pole-to-ground (n-g) fault applied at F2. As can be seen from this figure, none of the protection units located on Bases 1 and 3 has been activated during the severe n-g fault on Line 13. In other words, the protection of the positive pole of Line 13 has remained stable during the n-g fault on the same line.

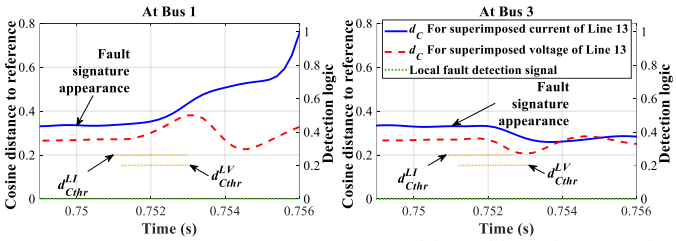

Fig. 13. Cosine distances and detection signals of the positive pole's protection for a solid n-g fault at F2, in the modified bipolar grid.

TABLE II
Comparison of the Proposed Scheme with Existing Ones

Line protection	Sampling frequency	Maximum detected fault resistance
Scheme of [5]	Not declared	Not declared
Scheme of [6]	100 kHz	60 Ω
Scheme of [7]	100 kHz	400 Ω
Scheme of [8]	20 kHz	200 Ω
Scheme of [9]	Not declared	200 Ω
Scheme of [10]	10 kHz	300 Ω (single-pole) 750 Ω (pole-to-pole)
Scheme of [11]	20 kHz	200 Ω
Scheme of [12]	96 kHz	500 Ω
Scheme of [13]	1000 kHz	300 Ω
Scheme of [14]	25 and 100 kHz	500 Ω
Scheme of [15]	50 kHz	10 Ω (backup)
Scheme of [16]	200 kHz	300 Ω
Scheme of [18]	10 kHz	1000 Ω (backup)
Scheme of [19]	100 kHz	300 Ω
Scheme of [20]	5 kHz	300 Ω
Scheme of [21]	Not declared	380 Ω (primary) 1000 Ω (backup)
Scheme of [22]	50 kHz	400 Ω (backup)
Scheme of [23]	1000 kHz	150 Ω
Proposed scheme	5 kHz	500 Ω (single-pole) 1000 Ω (pole-to-pole)

G. Comparison with Existing Methods

Table II compares the proposed scheme to the existing

protections of lines in MMC-HVDC grids. As can be seen in this table, compared to the primary protections, the proposed protection can detect higher-resistance faults. Only the backup protections presented in [18] and [21] have demonstrated the ability in detecting faults with a high resistance of 1000 Ω.

It should be noted that a lower sampling frequency increases the time between samples; consequently, it provides more time for real-time computations and facilitates the implementation of the protection algorithm. Based on Table II, the proposed method requires the lowest sampling frequency compared to other methods. Although the required sampling frequency of the scheme presented in [20] is also 5 kHz, this scheme needs distributed measurements along lines and has shown lower capability in detecting high-resistance faults compared to the proposed scheme.

V. Conclusion

A new scheme has been presented for protecting lines of half-bridge MMC-HVDC grids. This scheme is based on the cosine distance of the superimposed signals relative to the corresponding prerecorded samples. The proposed scheme's performance has been evaluated in a test grid. The results have confirmed that this scheme is highly sensitive to internal line faults, and it can detect them and issue trip commands very fast, even in the presence of a reasonable level of measurement errors. Furthermore, the scheme is absolutely robust against external faults outside the protected line and does not operate incorrectly. Among the advantages of this scheme, its low sampling frequency requirement of 5 kHz and high capability in detecting high-resistance internal faults can be emphasized.

References

[1] K. Sharifabadi, L. Harnefors, H.-P. Nee, S. Norrga, and R. Teodorescu, *Design, Control, and Application of Modular Multilevel Converters for HVDC Transmission Systems*. Chichester, West Sussex, United Kingdom: Wiley-IEEE Press, 2016.

[2] M. Hajian, L. Zhang, and D. Jovcic, "DC transmission grid with low-speed protection using mechanical DC circuit breakers," *IEEE Trans. Power Del.*, vol. 30, no. 3, pp. 1383-1391, Jun. 2015.

[3] D. Jovcic, W. Lin, S. Nguefeu, and H. Saad, "Low-energy protection system for DC grids based on full-bridge MMC converters," *IEEE Trans. Power Del.*, vol. 33, no. 4, pp. 1934-1943, Aug. 2018.

[4] S. Du, A. Dekka, B. Wu, and N. Zargari, *Modular Multilevel Converters: Analysis, Control, and Applications*. Hoboken, New Jersey, United States: Wiley-IEEE Press, 2018.

[5] J. Sneath and A. D. Rajapakse, "Fault detection and interruption in an earthed HVDC grid using ROCOV and hybrid dc breakers," *IEEE Trans. Power Del.*, vol. 31, no. 3, pp. 973-981, Jun. 2016.

[6] W. Leterme, J. Beerten, and D. V. Hertem, "Nonunit protection of HVDC grids with inductive DC Cable termination," *IEEE Trans. Power Del.*, vol. 31, no. 2, pp. 820-828, Apr. 2016.

[7] Q. Huang, G. Zou, X. Wei, C. Sun, and H. Gao, "A non-unit line protection scheme for MMC-based multi-terminal HVDC grid," *Int. J. Elec. Power*, vol. 107, pp. 1-9, May 2019.

[8] W. Xiang, S. Yang, L. Xu, J. Zhang, W. Lin, and J. Wen, "A Transient voltage-based DC fault line protection scheme for MMC-based DC grid embedding DC breakers," *IEEE Trans. Power Del.*, vol. 34, no. 1, pp. 334-345, Feb. 2019.

[9] S. Yang, W. Xiang, R. Li, X. Lu, W. Zuo, and J. Wen, "An improved DC fault protection algorithm for MMC HVDC grids based on modal domain analysis," *IEEE J. Emerg. Sel. Top. Power Electron.*, p. 13, to be published, 2020.

[10] L. Sabug, A. Musa, F. Costa, and A. Monti, "Real-time boundary wavelet transform-based DC fault protection system for MTDC grids," *Int. J. Elec. Power*, vol. 115, Feb. 2020.

[11] S. Jamali and S. S. Mirhosseini, "Protection of transmission lines in multi-terminal HVDC grids using travelling waves morphological gradient," *Int. J. Elec. Power*, vol. 108, pp. 125-134, Jun. 2019.

[12] M. Ikhide, S. B. Tennakoon, A. L. Griffiths, H. Ha, S. Subramanian, and A. J. Adamczyk, "A novel time domain protection technique for multi-terminal HVDC networks utilising travelling wave energy," *Sustain. Energy Grids*, vol. 16, pp. 300-314, Dec. 2018.

[13] L. Tang, X. Dong, S. Shi, and Y. Qiu, "A high-speed protection scheme for the DC transmission line of a MMC-HVDC grid," *Electr. Pow. Syst. Res.*, vol. 168, pp. 81-91, Mar. 2019.

[14] S. Zhang, G. Zou, C. Wang, J. Li, and B. Xu, "A non-unit boundary protection of DC line for MMC-MTDC grids," *Int. J. Elec. Power*, vol. 116, Mar. 2020.

[15] J. Sun, M. Saeedifard, and A. P. S. Meliopoulos, "Backup protection of multi-terminal HVDC grids based on quickest change detection," *IEEE Trans. Power Del.*, vol. 34, no. 1, pp. 177-187, Feb. 2019.

[16] N. Tong, X. Lin, Y. Li, Z. Hu, N. Jin, F. Wei, and Z. Li, "Local measurement-based ultra-high-speed main protection for long distance VSC-MTDC," *IEEE Trans. Power Del.*, vol. 34, no. 1, pp. 353-364, Feb. 2019.

[17] W. Leterme, M. Barnes, and D. V. Hertem, "Signal processing for fast fault detection in HVDC grids," *CSEE J. Power Energy Syst.*, vol. 4, no. 4, pp. 469-478, Dec. 2018.

[18] Y. Wang, Z. Hao, B. Zhang, and F. Kong, "A pilot protection scheme for transmission lines in VSC-HVDC grid based on similarity measure of traveling waves," *IEEE Access*, vol. 7, pp. 7147-7158, 2019.

[19] A. E. B. Abu-Elanien, A. A. Elserougi, A. S. Abdel-Khalik, A. M. Massoud, and S. Ahmed, "A differential protection technique for multi-terminal HVDC," *Electr. Pow. Syst. Res.*, vol. 130, pp. 78-88, Jan. 2016.

[20] D. Tzelepis, A. Dyśko, G. Fusiek, J. Nelson, P. Niewczas, D. Vozikis, P. Orr, N. Gordon, and C. D. Booth, "Single-ended differential protection in MTDC networks using optical sensors," *IEEE Trans. Power Del.*, vol. 32, no. 3, pp. 1605-1615, Jun. 2017.

[21] C. Li, A. M. Gole, and C. Zhao, "A fast DC fault detection method using DC reactor voltages in HVDC grids," *IEEE Trans. Power Del.*, vol. 33, no. 5, pp. 2254-2264, Oct. 2018.

[22] Q. Huang, G. Zou, S. Zhang, and H. Gao, "A pilot protection scheme of DC lines for multi-terminal HVDC grid," *IEEE Trans. Power Del.*, vol. 34, no. 5, pp. 1957-1966, Oct. 2019.

[23] Y. Li, Y. Gong, and B. Jiang, "A novel traveling-wave-based directional protection scheme for MTDC grid with inductive DC terminal," *Electr. Pow. Syst. Res.*, vol. 157, pp. 83-92, Apr. 2018.

[24] D. J. Weller-Fahy, B. J. Borghetti, and A. A. Sodemann, "A survey of distance and similarity measures used within network intrusion anomaly detection," *IEEE Commun. Surv. Tutor.*, vol. 17, no. 1, pp. 70-91, First quarter 2015.

[25] W. Leterme, N. Ahmed, J. Beerten, L. Ängquist, D. V. Hertem, and S. Norrga, "A new HVDC grid test system for HVDC grid dynamics and protection studies in EMT-type software," in *11th IET Int. Conf. on AC and DC Power Transmission*, 2015, pp. 1-7.

[26] Y. Serizawa, M. Myoujin, S. Miyazaki, and K. Kitamura, "Transmission delay variations in OPGW and overhead fiber-optic cable links," *IEEE Trans. Power Del.*, vol. 12, no. 4, pp. 1415-1421, Oct. 1997.

[27] M. Farshad, "Ultra-high-speed non-unit non-differential protection scheme for buses of MMC-HVDC grids," *IET Renew. Power Gener.*, p. 11, to be published, 2020.